# Imaging of cancer by redox-mediated mechanism: a radical diagnostic approach†

Zhivko Zhelev,[a] Rumiana Bakalova,*[a] Ichio Aoki,[a] Veselina Gadjeva[b] and Iwao Kanno[a]

*Received 23rd July 2010, Accepted 23rd August 2010*
DOI: 10.1039/c0mb00113a

**The present study describes a new diagnostic approach for carcinogenesis based on the different tissue redox activity of normal and cancer-bearing mammalians and its visualization and estimation by cell permeable and DNA annealing probe (nitroxide-labeled nitrosourea) and magnetic resonance imaging.**

In the July 2009 issue of *Nature Reviews Drug Discovery*, Trahootham *et al.* have summarized the advanced concepts about the role of reactive oxygen species (ROS) in carcinogenesis and cancer therapy.[1] Over 50 years experience in free radical biology and medicine shows that the normal cells of healthy mammalians are characterized with low steady-state level of ROS and some constant (referent) level of reducing equivalents (RE) (Fig. 1S, ESI†). Increasing ROS above the critical level provokes genomic instability and uncontrolled proliferation. The normal cells become malignant. The rapidly proliferative cancer cells require a lot of energy, which is accompanied by abnormal production and consumption of RE. On the other hand, the ROS in cancer cells have to be kept below the threshold level for induction of apoptosis and cell death, which is accompanied by antioxidant consumption. The substances necessary for energy production and proliferation, as well as the antioxidants in cancer are provided by the normal tissues of cancer-bearing mammalians. These "normal" tissues become deficient in antioxidants and RE, while the level of ROS in them is over the referent level characteristic for healthy mammalians. The conclusion is that the levels of ROS and RE are rather different in cancer and normal tissues and the abnormal generation of ROS provokes genomic instability and cancer development, which could be a key to the successful cancer therapy.

It is widely accepted that the balance between ROS and RE in cells and tissues determines their redox activity. Our study is directed to imaging of carcinogenesis by redox-mediated mechanism. We are assuming that the redox activities of normal (healthy) and cancer tissues are different and this parameter could be used as a diagnostic marker for carcinogenesis and a prognostic marker for the efficiency of cancer therapy.

Currently, there is no universal non-invasive methodology for estimation of ROS/RE balance and, respectively, for estimation of tissue redox activity in intact mammalians. In cells and tissues, the total ROS level is determined by the levels of superoxide radicals, hydrogen peroxide, nitric oxide radicals, end-products of lipid peroxidation, natural antioxidants, enzymatic antioxidant systems, *etc.* The total RE level is determined by the status of the endogenous redox pairs: $NADH/NAD^+$, $NADPH/NADP^+$, reduced/oxidized glutathione, reduced/oxidized ascorbic acid, *etc.* Each parameter is estimated separately.[1–6] The difference between ROS/RE balance of cancer and normal tissues are based on comparative analysis of one or several of these parameters and the conclusions are usually controversial.[1–6]

In the present study we propose a new approach for non-invasive imaging of tissue redox activity in intact healthy and cancer-bearing mammalians, which allows a differentiation of cancer development from normal (healthy) condition.

The method is based on redox cycle of nitroxide probes and their MRI contrast properties, which makes them useful molecular sensors for tissue redox activity (Fig. 1). The nitroxide radical (which is characterized by $T_1$ contrast properties) participates in electron-transfer reactions with ROS and RE with formation of non-contrast intermediate products (hydroxylamine and oxoammonium ion).[7–10] The rate constants of these reactions determine the MRI signal decay of nitroxide probe in living cells and tissues. In healthy mammalians, the half-life of MRI signal decay ($\tau_{1/2}$) in the selected region of interest (ROI; for example, brain tissue) could be considered as a reference steady-state level of tissue redox activity in norm. We supposed that in cancer-bearing mammalians, the half-life of MRI signal decay in the same or similar ROI has to be different from this reference level.

In our previous study we demonstrated that only *cell-permeable* nitroxide probes are appropriate for tissue redox imaging.[11,12] ROS and RE are predominantly produced and localized into the cells. Therefore, the probe is required to enter the cell to be able to interact with ROS and RE.

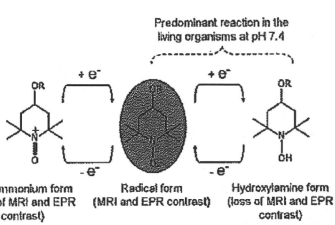


**Fig. 1** Redox cycle of nitroxide radical and its MRI and EPR contrast properties.

[a] *Department of Biophysics, Molecular Imaging Center, NIRS, 4-9-1 Anagawa, Inage-ku, Chiba 263-8555, Japan. E-mail: bakalova@nirs.go.jp, ra_bakalova@yahoo.com; Fax: +81-43-206-3276; Tel: +81-43-206-4067*
[b] *Department of Chemistry and Biochemistry, Thrakia University, Stara Zagora, Bulgaria*

† Electronic supplementary information (ESI) available. Experimental details and supplementary figures. See DOI: 10.1039/c0mb00113a

In the present study, we used nitroxide-labeled nitrosourea (SLENU)—a cell-permeable and DNA annealing probe (Fig. 2S, ESI†). SLENU is a nitroxide-labeled analogue of the conventional anticancer drug CCNU (Lomustine).[13] LD50 (in mice) for SLENU was ~100 mg $kg^{-1}$ b.w. *vs.* ~56 mg $kg^{-1}$ b.w. for CCNU.[12] In the present study, SLENU was applied in 0.2–0.4 mmol $kg^{-1}$ b.w. (single injection), which is below the LD50 value. In our previous studies, we established that the anticancer effect of SLENU is similar to that of CCNU.[12,13]

The animals (Balb6 nude mice) were separated in two groups: healthy mice (controls; $n = 6$) and mice with brain neuroblastoma (cancer-bearing mice; $n = 7$). In both groups, the mice were same age, almost same weight (~25 g), and kept under same conditions. Neuro2a cells ($0.5 \times 10^5$ cells in 10 μL) were inoculated in one hemisphere of the brain and the MRI measurements were performed on the 7th–8th day after inoculation. Neuro2a cells initiate a development of brain neuroblastoma without significant angiogenesis within ~10 days after inoculation (Fig. 3S, ESI†). It allows us to ignore the MRI signal of nitroxide coming from the blood vessels, which is not indicative for tissue redox activity. Thus, the MRI signal of nitroxide probe in the tumor area could be considered as a result of its permeability and localization in the cancer cells.

The MRI measurements were performed on 7 tesla MRI. $T_1$-weighted incoherent gradient-echo sequence (fast low-angle shot; FLASH) was used (details are described in the ESI†). The animal was under anesthesia (1.5% isoflurane). The tail vein was canulated for drug administration. The MR imaging of mouse brain was started. After the 5th frame (scan-time ~1 min 40 s) during continuous scanning, the nitroxide was injected (100 μL per 25 g b.w.; single fast injection, within 15–20 s) and the MR imaging continued up to 40 frames (total scan-time ~14 min). Two ROI were selected: brain tissue (cortex) and soft tissues surrounding the brain (Fig. 3S, ESI†).

Fig. 2A shows a typical kinetics of MRI signal enhancement by SLENU in the brain of control mouse. The signal increased slightly after injection, followed by rapid decay. The first 5 frames (before injection of SLENU) were used for calculation of the averaged baseline level. All data were normalized to the baseline. The data were processed with *ImajeJ* software. The histograms in Fig. 2B represent the normalized data from 6 animals. The profiles of these histograms could be considered as reference profiles for the normal (healthy) condition of the respective tissue. In control mice, the half-life of MRI signal decay was about 1 min or 2 min 20 s in the brain or surrounding tissues, respectively. These $\tau_{1/2}$ values could be considered as reference values for the normal redox activity of the respective tissues. The profile of the histograms and $\tau_{1/2}$ values in Fig. 2 are indicative of a high reducing activity of the brain and surrounding tissues to the injected nitroxide radical.

In cancer-bearing mice, the profiles of time-dependent MRI signal enhancement by SLENU in the brain and surrounding tissues (Fig. 3) were completely different from that of the reference profiles, detected in control mice (Fig. 2B). The MRI signal intensity increased after the injection of nitroxide and remained high and stable over 14 min, without decay (Fig. 3A). In this case, the half-life of MRI signal decay can be considered over 14 min.

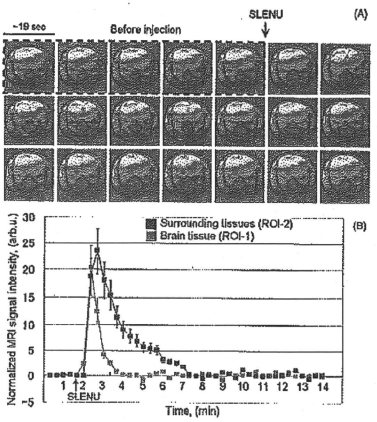


Fig. 2 (A) Time-dependent MR images (gradient-echo sequence) of the brain of normal (healthy) mouse before and after injection of SLENU. (B) MRI signal enhancement by SLENU in the brain (ROI-1) and surrounding tissues (ROI-2) under continuous scanning within 14 min. The data are mean ± SEM from 6 animals.

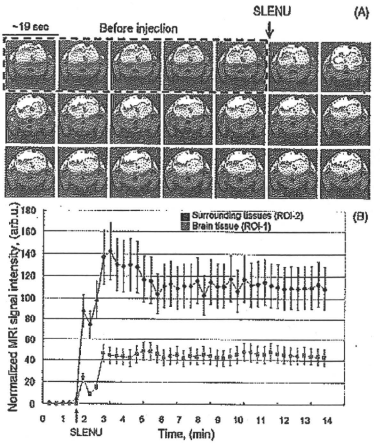


Fig. 3 (A) Time-dependent MR images (gradient-echo sequence) of the brain of cancer-bearing mouse before and after injection of SLENU. (B) MRI signal enhancement by SLENU in the brain (ROI-1) and surrounding tissues (ROI-2) under continuous scanning within 14 min. The data are mean ± SEM from 7 animals.

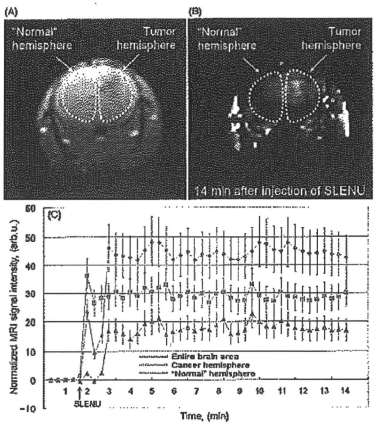


Fig. 4 (A) MR image (gradient-echo sequence) of tumor in mouse brain obtained 8 days after inoculation of cancer cells in Balb6 nude mouse. (B) Extracted MRI signal enhancement by SLENU, obtained 14 min after injection. The dotted lines indicate ROI—cancer hemisphere and "normal" hemisphere of the brain. (C) MRI signal enhancement by SLENU in the entire brain area, cancer hemisphere and "normal" hemisphere under continuous scanning within 14 min. The data are mean ± SEM from 4 animals.

In cancer-bearing mice, the profiles of the histograms were same in the cancer hemisphere of the brain, "normal" (non-cancer) hemisphere, and "normal" surrounding tissues (Fig. 4C). These profiles and $\tau_{1/2}$ values are indicative of a low reducing activity of the brain and surrounding "normal" tissues of cancer-bearing animals to the nitroxide probe. The "normal" tissues around the tumor have a different metabolic activity from the pre-cancer state, making them more sensitive to oxidation and damage.

Fig. 4b demonstrates the extracted MRI signal enhancement by SLENU from the original image, normalized to the baseline signal. It is well-seen that SLENU (as DNA annealing substance) is accumulated into the cancer tissue and the MRI signal is very high within 14 min after injection.

In a separate experiment *in vitro* using EPR spectroscopy, we investigated the amount of SLENU in extracted brain tissue after perfusion by saline solution. The brain was extracted ~5–10 min after injection of SLENU in the tail vein. The tissue homogenates were incubated with ferricyanide within 15 min. The ferricyanide quantitatively converts the reduced (non-EPR contrast) nitroxide to the oxidized (EPR contrast) radical form (Fig. 1). All tissue homogenates were treated at same conditions. Equal amounts of SLENU were detected in the brain of control mice and cancer-bearing mice—6.7 ± 1.2 pmol per mg tissue and 7.1 ± 0.9 pmol per mg tissue, respectively. Therefore, it can be concluded that the different MRI signal intensity and dynamics of SLENU in the brain of healthy and cancer-bearing mice is not a result of the different nitroxide concentration in the brain tissue. The different MRI signal dynamics of normal (healthy) and cancer tissues is a result of their different redox activity to the nitroxide radical.

In conclusion, the present study demonstrates a development of new diagnostic approach for carcinogenesis based on the different tissue redox activity of normal and cancer-bearing mammalians and its imaging by cell permeable nitroxide SLENU and MRI. There is a very clear difference between MRI signal enhancement by SLENU in healthy and cancer-bearing brain, which is indicative of the different metabolic activity of both tissues. In this case, the half-life of MRI signal decay is an appropriate diagnostic marker for carcinogenesis and a prognostic marker for the efficiency of cancer therapy. The described methodology is also applicable in isolated tissue specimens (*e.g.*, biopsy specimens).

This study also demonstrates that the piperidine-type nitroxide radical possesses a high contrast for MR imaging *in vivo* and this contrast is highly sensitive to the tissue redox activity.

## Acknowledgements

The technical support of Ms Sayaka Shibata and Mr Shigeyoshi Saito (Molecular Imaging Center, NIRS-Chiba, Japan) are gratefully acknowledged. This study was partially supported by the JSPS through its "Funding Program for World-Leading Innovative R&D on Science and Technology" and Grand-in-aid "Kakenhi" No 21611011

## References

1 D. Trachootham, J. Alexandre and P. Huang, *Nat. Rev. Drug Discovery*, 2009, **8**, 579.
2 J. Fang, T. Seki and H. Maeda, *Adv. Drug Delivery Rev.*, 2009, **61**, 290.
3 T. W. Miller, J. S. Isenberg and D. D. Roberts, *Chem. Rev.*, 2009, **109**, 3099.
4 J. R. Kanwar, R. K. Kanwar, H. Burrow and S. Baratchi, *Curr. Med. Chem.*, 2009, **16**, 2373.
5 G. Pani, E. Giannoni, T. Galeotti and P. Chiarugi, *Antioxid. Redox Signaling*, 2009, **11**, 2791.
6 M. Landriscina, F. Maddalena, G. Laudiero and F. Esposito, *Antioxid. Redox Signaling*, 2009, **11**, 2701.
7 G. M. Rosen, M. S. Cohen, B. E. Britigan and S. Pou, *Free Radical Res.*, 1990, **9**, 187.
8 B. P. Soule, F. Hyodo, K. Matsumoto, N. L. Simone, J. A. Cook, M. C. Krishna and J. B. Mitchell, *Antioxid. Redox Signaling*, 2007, **9**, 1731.
9 F. Hyodo, B. P. Soule, K. Matsumoto, S. Matsumoto, J. A. Cook, E. Hyodo, A. L. Sowers, M. C. Krishna and J. B. Mitchell, *J. Pharm. Pharmacol.*, 2008, **60**, 1049.
10 J. Trnka, F. H. Blaikie, R. A. Smith and M. P. Murphy, *Free Radical Biol. Med.*, 2008, **44**, 1406.
11 Z. Zhelev, R. Bakalova, I. Aoki, K. Matsumoto, V. Gadjeva, K. Anzai and I. Kanno, *Chem. Commun.*, 2009, (1), 53.
12 Z. Zhelev, R. Bakalova, I. Aoki, K. Matsumoto, V. Gadjeva, K. Anzai and I. Kanno, *Mol. Pharmaceutics*, 2009, **6**, 504.
13 V. Gadjeva, *Eur. J. Med. Chem.*, 2002, **37**, 295.

J Physiol Sci (2010) 60:399–406
DOI 10.1007/s12576-010-0108-9

ORIGINAL PAPER

# Contribution of nitric oxide to cerebral blood flow regulation under hypoxia in rats

Hiroyuki Takuwa · Tetsuya Matsuura · Romiana Bakalova · Takayuki Obata · Iwao Kanno

Received: 21 March 2010 / Accepted: 2 August 2010 / Published online: 7 October 2010


Abstract This study was designed to clarify whether nitric oxide (NO) participates in the regulation of local cerebral blood flow (CBF) during hypoxia (inhalation of 15% $O_2$ in $N_2$). The CBF response to hind-paw stimulation (evoked CBF) of Sprague-Dawley (SD) rats was measured by laser-Doppler flowmetry. Physiological variables, such as heart rate, mean blood pressure, and $PaCO_2$ during hypoxia, were identical to those under normoxic conditions. Hypoxia increased the baseline CBF (17.5 ± 14.3%) and the normalized peak amplitude of evoked CBF (31.1 ± 18.5%) relative to those during normoxia. When an NOS inhibitor was infused intravenously, these differences were abolished in both the baseline CBF or evoked CBF between normoxic and hypoxic conditions, whereas the heart rate decreased and the mean blood pressure increased during hypoxia in comparison with these during normoxia. The field potential was constant under all experimental conditions. These results suggest that NO plays a major role in the regulation of baseline and evoked CBF during hypoxia.

Keywords Cerebral blood flow · Functional activation · Laser-Doppler flowmetry · Somatosensory stimulation · Rat · Nitric oxide

H. Takuwa (✉) · T. Matsuura · R. Bakalova · T. Obata · I. Kanno
Department of Biophysics, Molecular Imaging Center, National Institute of Radiological Sciences, 4-9-1 Anagawa, Chiba 263-8555, Japan
e-mail: takuwa@nirs.go.jp

T. Matsuura (✉)
Academic Group of Mathematical and Natural Science, Iwate University, 4-3-5 Ueda, Morioka 020-8551, Japan
e-mail: matsuura@iwate-u.ac.jp

## Introduction

Changes in local cerebral blood flow (CBF) are closely related to neural activity; therefore, the cerebral hemodynamic response has been used extensively to map brain function in humans and animals. One of the major roles of CBF is to supply oxygen to the brain tissues. The relationship between oxygen metabolism and CBF is of considerable interest to many researchers.

In the case of baseline CBF, it has been reported that an increased arterial oxygen supply (hyperoxia) results in a decrease in the baseline level of CBF in rats [1], whereas a decreased arterial oxygen supply (hypoxia) increases the baseline level of CBF in humans [2] and in the somatosensory cortex of rats [3–5]. These observations indicate that the baseline CBF is affected by the $O_2$ level in the supplying blood in brain tissue.

On the other hand, in the case of an increase in local CBF (evoked CBF), induced by neuronal activation, the relationship between evoked CBF and blood oxygenation in the activated brain area is still a disputable and controversial issue. In our previous study, we reported that hyperoxia provokes the enhancement of evoked CBF in the V1 area of the human brain [6, 7] and in the somatosensory cortex of rats [1]. In a human study, using positron emission tomography (PET), Mintun et al. [2] reported that hypoxia does not enhance evoked CBF, suggesting that evoked CBF is independent of the oxygen supply or metabolic demand. In contrast, several studies in rats, using functional magnetic resonance imaging (fMRI) and optical spectroscopy, showed that hyperoxia provokes a decrease in evoked CBF, while hypoxia induces its enhancement [3, 4, 8]. These studies suggest that evoked CBF depends on the oxygen metabolic demand.

The dynamics of the evoked CBF is highly complicated and many biochemical mediators could be considered in

the regulation system, such as nitric oxide (NO), cyclo-oxygenase-1 (COX-1), COX-2, and adenosine [9–11]. NO, produced by endothelial and neuronal nitric oxide synthase (NOS), acts as a neurotransmitter and is involved in the regulation of cerebral circulation. In particular, it is also an important mediator of the cerebral vasodilatation in response to changes in the physiological parameters during hypercapnia [12] and hyperoxia [1]; however, the role of NO in evoked CBF regulation remains to be elucidated. In our previous study, we reported that the NOS inhibition was accompanied by a decrease in baseline CBF during normoxia and suppression of evoked CBF during hyperoxia [1]. We speculated that NOS inhibition would also suppress the effect of hypoxia on cerebral circulation.

In the present study, we investigated the effect of hypoxia on the baseline levels of CBF and evoked CBF using laser-Doppler flowmetry (LDF) to clarify the regulation mechanism of CBF in relation to the metabolic oxygen demand. The effect of NOS inhibition on CBF regulation under hypoxia was also demonstrated using $N^{\omega}$-nitro-L-arginine (LNA) as a pharmacological tool.

## Materials and methods

### Animal preparation and control of physiological conditions

All experiments were conducted in accordance with the guidelines of the Physiological Society of Japan and were approved by the Animal Care and Use Committee of the National Institute of Radiological Sciences, Chiba, Japan.

Sprague-Dawley rats (370–420 g) were anesthetized with isoflurane (4% for induction and 1.5% during surgery) in 30% $O_2$ and 70% $N_2$ using a face mask. Subcutaneous 2% lidocaine was used before incision to prevent vasospasm during catheter insertion. The tail artery and left femoral vein were cannulated for blood pressure monitoring, blood gas sampling, and intravenous drug administration. After tracheotomy, α-chloralose (75 mg/kg body weight, i.v.) was administered and isoflurane administration was discontinued. Anesthesia was maintained with α-chloralose (44 mg/kg/h, i.v.), and muscle relaxation was maintained with pancuronium bromide (0.7 mg/kg/h, i.v.) during the experimental period. Body temperature was monitored with a rectal probe and maintained at approximately 37.0°C using a heating pad (ATC-210; Unique Medical, Japan). The rat was fixed in a stereotactic frame, and the parietal bone was thinned to translucency at the left somatosensory cortex using a dental drill (an area 3 × 3 mm, centered 2.5 mm caudal and 2.5 mm lateral to the bregma). To ensure a stable physiological condition of the animal, the measurements were performed 3 h after the preparation of the parietal bone (Fig. 1).

The rat was paralyzed by injection of pancuronium bromide and artificially ventilated using a respirator (SN-480-7; Shinano, Japan) with a mixture of $N_2$ and $O_2$ to achieve physiological arterial blood levels of $O_2$ and $CO_2$ tension ($PaO_2$ and $PaCO_2$, respectively). During the experiments, the changes in respiratory $O_2$ and $CO_2$ concentrations were monitored with a capnometer (SurgiVet V9004, Smiths Medical, USA). Arterial blood pressure

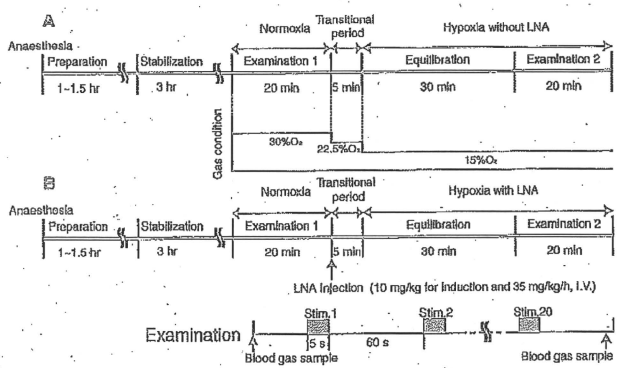


Fig. 1 Experimental protocol of hypoxia a without LNA (experiment A) and b hypoxia with LNA (experiment B). The experiment was carried out approximately 3 h after the preparation of rats. The evoked CBF and field potential were measured under normoxia, hypoxia without LNA, and hypoxia with LNA. In each examination, 20 successive stimuli (5 Hz and 5 s) were applied at 60 s intervals. The animals were ventilated with a 30% $O_2$ and 70% $N_2$ mixture during normoxia (control). To avoid a change in arterial blood pressure, the $O_2$ concentration was gradually decreased in a stepwise manner from 30 to 22.5 and 15% during hypoxia

Table 1 Physiological variables

| Condition | Heart rate (b.p.m.) | MABP (mmHg) | $PaCO_2$ (mmHg) | $PaO_2$ (mmHg) |
|---|---|---|---|---|
| (A) Protocol A ($n = 9$)[a] | | | | |
| Normoxia | 379.4 ± 40.6 | 88.8 ± 7.7 | 36.9 ± 2.3 | 93.3 ± 11.0 |
| Hypoxia without LNA | 403.4 ± 35.0 | 92.3 ± 8.2 | 34.9 ± 1.9 | 49.8 ± 3.0 * |
| (B) Protocol B ($n = 8$)[a] | | | | |
| Normoxia | 360.3 ± 19.7 | 98.0 ± 11.0 | 35.9 ± 2.3 | 101.8 ± 11.9 |
| Hypoxia with LNA | 315.3 ± 30.3 * | 134.6 ± 4.6 * | 36.9 ± 1.2 | 48.1 ± 1.4 * |

[a] Number of rats; mean ± SD

* $P < 0.01$

from the tail artery was measured with a pressure sensor (TP400T; Nihon Kohden, Japan) and recorded continuously using MacLab data acquisition software (AD Instruments, Australia) during the experiments; the mean arterial blood pressure (MABP) was calculated as the average at three time points (i.e., before, during, and immediately after each stimulation period). Arterial blood samples were serially collected before and immediately after each step of the experiment and analyzed for gas values.

### Baseline and evoked CBF measurements

The evoked CBF was measured by LDF (FLO-C1; OMEGA FLO) equipped with a probe with a tip diameter of 0.55 mm (Probe NS; OMEGA FLO). The sampling volume for the LDF measurement was approximately 1 $mm^3$ [13]. A time constant of 0.1 s was used to detect the LDF signal. The LDF probe was positioned over the thinned skull (over the somatosensory area of the hind paw). Electrical hind paw stimulation was performed with two needle electrodes inserted subdermally into the right hind paw contralateral to the LDF probe. A current stimulus of 1.5 mA (0.1 ms pulse) was applied at 5 Hz frequency and 5 s duration. In each experiment, 20 successive stimuli were applied at 60 s intervals and accumulated using MacLab data acquisition software. These stimulus parameters did not cause any change in the systemic arterial blood pressure and heart rate during stimulation.

The evoked CBF response to somatosensory stimulation was investigated under three experimental conditions as follows: normoxia (17 rats), hypoxia without LNA (9 rats), and hypoxia with LNA (8 rats) (Fig. 1).

### Hypoxia and application of NOS inhibitor

Under normoxia (control), the animals were ventilated with a 30% $O_2$ and 70% $N_2$ mixture. Hypoxia was induced by decreasing the concentration of inspired $O_2$ to 15%. The acute change from 30% $O_2$ to 15% $O_2$ often caused mild hypotension, so the $O_2$ concentration was gradually decreased in a stepwise manner from 30 to 22.5% and 15% (Fig. 1). This stepwise hypoxia had no effect on arterial blood pressure (Table 1). In the "hypoxia without LNA" experiment (Fig. 1a), we first examined the evoked CBF under normoxia. The oxygen concentration was then decreased in a stepwise manner from 30 to 22.5% and 15%. After an equilibration time of 30 min, the evoked CBF was measured during hypoxia without LNA. In the "hypoxia with LNA" experiment (Fig. 1b), we also examined the evoked CBF under normoxia. LNA was then applied intravenously (10 mg $kg^{-1}$ for induction and 35 mg $kg^{-1}$ $h^{-1}$ during experiments), and the $O_2$ concentration was decreased in a stepwise manner from 30 to 22.5% and 15%. After an equilibration time of 30 min, evoked CBF responses were measured under hypoxia with LNA administration.

### Measurement of neuronal activity

To estimate the correlation between the change in evoked CBF and neuronal activation, field potentials were measured in both experiments: "hypoxia without LNA" (6 rats) and "hypoxia with LNA" (6 rats). A tungsten microelectrode (12 MΩ) was inserted into the somatosensory area of the hind paw through the thinned portion of the skull and fixed using dental cement. The tip of the electrode was set at a depth of approximately 0.5 mm from the surface of the cortex. An Ag-AgCl indifferent electrode was placed between the skull bone and scalp. Field potentials under normoxia, hypoxia without LNA, and hypoxia with LNA were recorded using the same time schedule as evoked CBF measurements (Fig. 1). Twenty successive signals of the field potential recordings were also accumulated using MacLab data acquisition software and were digitized at 100 Hz, which was the same frequency as that in our previous study [1, 11, 14]. The mean amplitude of the field potentials was calculated as the average of the negative components of each spike to evaluate the neuronal activity during stimulation [1, 14].

### Data analysis

The LDF signal was normalized towards the baseline level as percent changes from the baseline (normalized evoked

CBF). The rise time of the evoked CBF was defined as the time at the intersection of the extrapolated lines, which was drawn with the baseline on the response curve from 90 to 10% of the peak [15, 16]. The peak amplitude indicated the percent change from the baseline to the maximum evoked CBF. Values were statistically analyzed by Student's *t* test and presented as the mean ± SD.

## Results

### Physiological variables during hypoxia and LNA administration

The physiological variables (i.e., heart rate, MABP, and $PaCO_2$) during hypoxia without LNA were almost identical to those during normoxia (control) (Table 1). Only the $PaO_2$ value (49.8 ± 3.0 mmHg) was significantly different from that measured during normoxia ($PaO_2$ = 93.3 ± 11.0 mmHg) ($P < 0.01$).

The systemic administration of the NOS inhibitor LNA during hypoxia (hypoxia with LNA) significantly increased MABP and decreased the heart rate relative to those parameters during normoxia ($P < 0.01$). $PaO_2$ was significantly lower during hypoxia with LNA (48.1 ± 1.4 mmHg) than during normoxia (101.8 ± 11.9 mmHg) ($P < 0.01$). There was no clear change in the respiratory $CO_2$ concentration between normoxia and hypoxia (data not shown).

### Effects of hypoxia on CBF

During hypoxia (in the absence of LNA), the baseline level of CBF was significantly higher than that during normoxia ($P < 0.05$) (Fig. 2). As shown in Fig. 3a, hypoxia enhanced the normalized evoked CBF in comparison with normoxia. There was a significant difference in the peak amplitude of the normalized evoked CBF between the hypoxic condition (20.4 ± 7.4%) and normoxic condition (15.3 ± 5.4%) ($P < 0.05$) (Fig. 3b). The rise time of evoked CBF was 0.67 ± 0.22 s during hypoxia and 0.51 ± 0.30 s during normoxia, although no significant difference in the rise time between the two conditions was detected. Presumably, some mediators involved in vasodilatation enhance baseline and evoked CBF during hypoxia. In the subsequent experiments, we focused on NO as one of the possible candidates responsible for vasodilatation.

### Application of NOS inhibitor during hypoxia

The injection of NOS inhibitors (LNA) in rats subjected to hypoxia resulted in the same baseline CBF as that during normoxia (Fig. 2). The normalized evoked CBF during

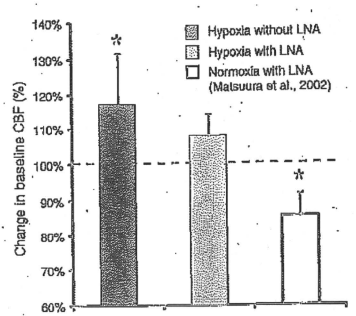


Fig. 2 Change in baseline CBF. The values of baseline CBF, obtained during normoxia, were considered to be 100%, indicated by *a dashed line*. *Black* and *gray bars* indicate the baseline CBF during hypoxia without LNA and hypoxia with LNA, respectively. The *white bar* indicates the baseline CBF during normoxia with LNA, which was obtained in the previous study [1]. The data were normalized to those under normoxia without LNA after statistical analysis. To evaluate the changes in baseline CBF, the absolute value of the baseline CBF was statistically compared for each animal group by paired *t* test. Note that the baseline CBF during hypoxia with LNA was not significantly different from that during normoxia, whereas the baseline CBF was higher during hypoxia without LNA than during normoxia. *Asterisks* indicate significant differences in levels of baseline CBF between hypoxia without LNA and normoxia without LNA, and normoxia with LNA and normoxia without LNA ($P < 0.05$). *Error bars* are SD

hypoxia with LNA did not increase in comparison with that during normoxia (Fig. 4b). The peak amplitude of the normalized evoked CBF was 22.8 ± 10.8% during normoxia and 19.5 ± 7.6% during hypoxia with LNA (Fig. 4c). A slight (but not significant) decrease in the evoked CBF was detected in rats subjected to hypoxia and with LNA. There was no significant difference in the rise time of evoked CBF between normoxia and hypoxia with LNA: 0.60 ± 0.23 s during hypoxia with LNA and 0.57 ± 0.29 s during normoxia. The results suggest that NO is involved in the enhancement of baseline and evoked CBF during hypoxia. The NO inhibitor abolished the effect of hypoxia completely at the baseline level and evoked CBF; therefore, NO could be considered as a major mediator of the relationship between hypoxia and evoked CBF response.

### Neural activities during experiments

Figure 5 shows one of the representative field potentials from the somatosensory cortex during normoxia, hypoxia without LNA, and hypoxia with LNA. The field potential during hypoxia without LNA was almost the same as that during normoxia (Fig. 5a). There were no significant differences in the mean amplitude and number of spikes of

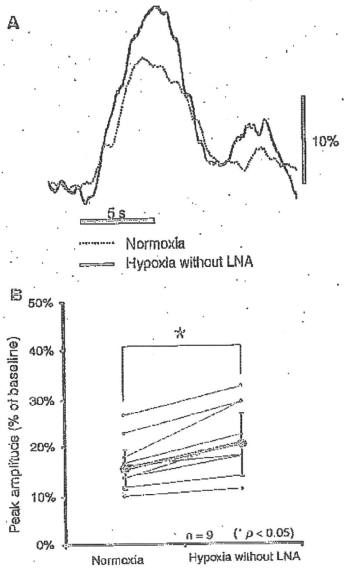


Fig. 3 Change in normalized evoked CBF under normoxia and hypoxia without LNA. a Normalized evoked CBF with somatosensory stimulation from one representative animal. Curves were normalized to the baseline level. *Horizontal* and *vertical bars* indicate the stimulation period and 10% increase from the baseline level, respectively. b Peak amplitude of normalized evoked CBF under normoxia and hypoxia without LNA. *Each line* corresponds to the data obtained from one rat. *Bold lines* and *error bars* indicate the mean value and SD, respectively ($n = 9$). Note that the normalized evoked CBF was significantly higher during hypoxia than during normoxia ($^*P < 0.05$)

field potentials between hypoxia without LNA and normoxia (Table 2). The results indicate that the enhancement of evoked CBF is not caused by an increase in neuronal activity during hind paw stimulation.

The field potential during hypoxia with LNA was also almost the same as that during normoxia (Fig. 5b). There were no significant differences in the mean amplitude and number of spikes of field potentials between hypoxia with LNA and normoxia (Table 2), indicating that the application of LNA did not affect neuronal activity.

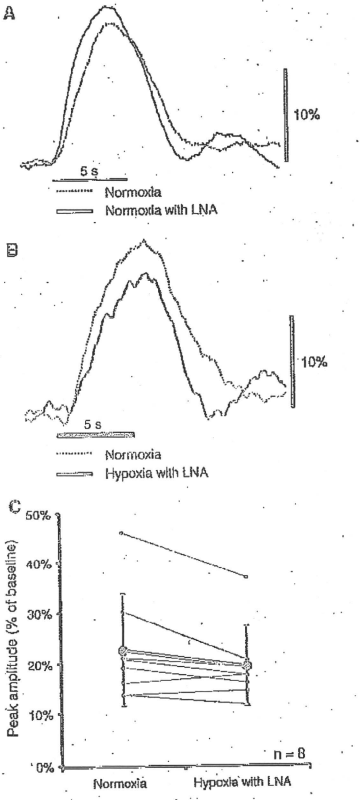


Fig. 4 Change in normalized evoked CBF during normoxia, normoxia with LNA, and hypoxia with LNA. a Normalized evoked CBF during normoxia without LNA and normoxia with LNA (cited from reference [1]). b Normalized evoked CBF during normoxia without LNA and hypoxia with LNA. Curves were normalized to the baseline level and shown for one representative animal. *Horizontal* and *vertical bars* indicate the stimulation period and 10% increase from baseline level, respectively. c Peak amplitude of normalized evoked CBF under normoxia and hypoxia with LNA. Each *line* corresponds to the data obtained from one rat. *Bold lines* and *error bars* indicate the mean value and SD, respectively ($n = 8$). No significant difference in the peak amplitude of normalized evoked CBF between normoxia and hypoxia with LNA was observed

## Discussion

In the present study, we investigated the effects of hypoxia on the regulation of baseline and evoked CBF in rats, as well as the role of NO in this relationship. NO is synthesized mainly by endothelial NOS (eNOS), neuronal NOS (nNOS), and inducible NOS (iNOS) in the brain tissue. To

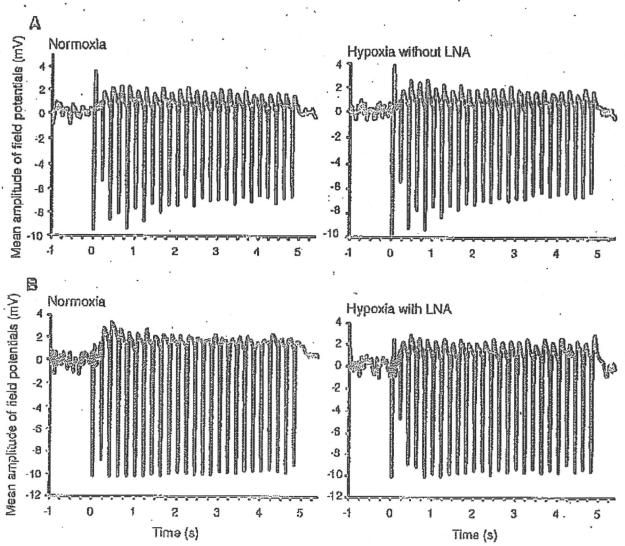


Fig. 5 Representative field potential recordings from the somatosensory cortex during hind paw stimulation. a Hypoxia without LNA. Neuronal activity during hypoxia without LNA was almost the same as that during normoxia. b Hypoxia with LNA. Field potential during hypoxia with LNA was almost identical to that during normoxia. In both experiments, there were no significant differences in the mean amplitude and number of spikes of field potentials between hypoxia and normoxia (see Table 2)

Table 2 Parameters of neuronal activity during each examination

| Condition | Mean amplitude of field potentials (mV) | | Number of spikes detected | |
|---|---|---|---|---|
| (A) Protocol A ($n = 6$)[a] | | | | |
| Normoxia | −4.3 ± 3.3 | NS | 20.8 ± 6.1 | NS |
| Hypoxia without LNA | −4.3 ± 3.5 | | 20.8 ± 6.1 | |
| (B) Protocol B ($n = 6$)[a] | | | | |
| Normoxia | −6.3 ± 2.3 | NS | 17.2 ± 5.8 | NS |
| Hypoxia with LNA | −6.4 ± 2.3 | | 17.2 ± 5.7 | |

Hind-paw stimulation (5 Hz and 5 s)

*NS* not significant

[a] Number of rats; mean ± SD

inhibit the activities of all these NOS isoenzymes, a non-selective NOS inhibitor, LNA, was used. A previous study showed that the intracortical administration of the NOS inhibitor affected the CBF during hypoxia [17]. We also found that the NOS inhibitor LNA infused intravenously attenuated the CBF response to hyperoxic conditions [1]. The intravenous infusion of LNA may cause excess accumulations of the drug leading to unfavorable effects on the evoked CBF. However, we revealed that the systemic administration of LNA under normoxic condition (normoxia with LNA) did not affect the neuronal activity and normalized evoked CBF (Fig. 4a), although it caused a decline in the level of the baseline CBF (Fig. 2) [1]. The experimental protocol used in this study should not cause any side effects of the drug leading to the normalized evoked CBF.

It has been reported that hypoxia causes mild hypotension [4, 5]. In our experiment, we avoided a significant reduction of MABP during hypoxia by applying a stepwise decrease in the inspired $O_2$ concentration and mild hypoxia (15% $O_2$) (Fig. 1). The other physiological parameters (i.e., heart rate and $PaCO_2$) during hypoxia were identical to those during normoxia (Table 1), which is in agreement with the previous report [5]. It is known that hypoxia activates distinct cellular and molecular processes in the brain depending on both its severity and time course (e.g., rate of decrease in oxygen tension and duration). The protocol in the hypoxia experiment was targeting $PaO_2$ within 40–50 mmHg, which was consistent with previous studies [3–5], but kept the $PaCO_2$, MABP, and heart rate within the normal range. The stepwise method of hypoxia used in this study is one of the best ways to achieve this and did not cause any serious damage to the brain tissue. Moreover, the inhalation of 15% $O_2$ in $N_2$ did not evoke a hypoxic ventilatory response (i.e., increases in minute ventilation) despite the fact that $PaO_2$ was significantly lowered (Table 1). In this study, rats were anesthetized and relaxed with continuous infusion of α-chloralose and pancuronium bromide during the experiment. Muscle relaxation with pancuronium bromide does not cause hypoxic ventilatory responses.

We reported that the baseline CBF was ~5.0% lower during hyperoxia than during normoxia [1], and we found in the present study that it was ~17.5% higher during hypoxia than during normoxia (Fig. 2). These results indicate that the baseline CBF under resting conditions is regulated to maintain a constant oxygen supply. The infusion of LNA in rats during hypoxia abolished the effect of hypoxia and returned the baseline to the level obtained during normoxia (Fig. 2). A decrease in the baseline CBF under normoxia with LNA has been reported (Fig. 2) [1]. Their results suggest that the systemic administration of LNA suppresses the NO activity and the decline in the baseline CBF. We considered that the increase in the baseline CBF during hypoxia was caused by an increase in the level of NO activity.

Mintun et al. [2] reported following a PET study that there is no significant difference in the normalized regional CBF response to visual stimulation between normoxia and hypoxia and that the baseline level of CBF is higher during hypoxia than during normoxia. The discrepancy between our findings and the results of the PET study might be a result of the differences in experimental protocols and measurement techniques. For example, the time resolution of LDF in this study is much higher than that of PET. A higher time resolution of LDF is feasible in detecting the detailed time course of evoked CBF during hypoxia. Thus, it is possible that an increase in evoked CBF during hypoxia could be detected in our present LDF study that might have been smoothed out in the PET study.

The peak amplitude of normalized evoked CBF is higher under hyperoxia than under normoxia [1, 7]. The normalized evoked CBF during hypoxia was also enhanced in comparison with that during normoxia (Fig. 3). These observations suggest that the evoked CBF is enhanced by abnormal oxygen supply, such as high and low levels of oxygen in the brain tissue. The peak amplitude of normalized evoked CBF during hypoxia with LNA was also the same as that during normoxia (Fig. 4b). We previously reported that LNA administration during hyperoxia decreased not only evoked CBF but also the neural activity. Therefore, the increase in the evoked CBF during hyperoxia was not simply accounted for by the up-regulated NOS expression. On the other hand, there was no significant difference in neuronal activity between normoxia and hypoxia with LNA (Fig. 5; Table 2). These observations suggest that hypoxia is accompanied by an increase in NOS activity, and that LNA administration during hypoxia suppresses this process.

It has been reported that although the baseline CBF is higher during hypercapnia than that during normocapnia, there was no significant difference in normalized evoked CBF between the hypercapnic and normocapnic conditions [18]. These results indicated that the absolute value of evoked CBF increases according to the baseline CBF during hypercapnia; that is, the evoked CBF under hypercapnia is proportional to the baseline CBF. In contrast, we established that the normalized evoked CBF is higher during hypoxia than during normoxia despite the increase in baseline CBF (Fig. 3). This suggests that there are some differences in the mechanism of NOS activity between hypercapnia and hypoxia. Since hypoxia is accompanied by free radical generation in the hypoxic area [19], it may be speculated that nitric oxide radicals and their intermediate products are involved in the regulation of evoked CBF response during hypoxia, while hypercapnia is not accompanied by such free radical mechanism.

A previous study showed that the increase in neuronal activity induced by stimulation in rat was unchanged during acute hypoxia relative to that under normoxia [3]. As mentioned above, in the present study, hypoxia was caused by a stepwise mild decrease in the respiratory $O_2$ concentration. The neuronal activity was not significantly different between hypoxia and normoxia (Fig. 5; Table 2), suggesting that the neural activity induced by stimulation is stable during the experiment. The enhancement of evoked CBF during hypoxia in this study may be caused by a low oxygen supply level within the activated brain area.

It is well known that NO is a key mediator of cerebrovascular responses to carbon dioxide and involved in neurovascular coupling. However, the effects of NOS inhibitors, such as LNA, on the neurovascular coupling differ with each experimental condition. LNA by itself reduced the evoked CBF slightly but not completely. This is because the CBF response to neuronal activation is mediated by various mediators, e.g., NO, prostaglandins, adenosine, and ions [11, 16]. LNA blocks only NO synthesis, but not the effects of other mediators of neurovascular coupling. In our study, we observed that LNA abolished completely the effect of hypoxia on the evoked CBF response. Moreover, the evoked CBF response is slightly lower in the presence of LNA than under normoxia (Fig. 4). This means that a part of the evoked CBF response to normoxia, but not the total response, could be explained by the effect of NO.

**Acknowledgments** The present work was supported by a grant from the Ministry of Education, Culture, Sports, Science and Technology of Japan, and KAKENHI from the Japan Society for the Promotion of Science.

## References

1. Matsuura T, Kanno I (2002) Effect of nitric oxide synthase inhibitor on the local cerebral blood flow evoked by rat somatosensory stimulation under hyperoxia. Comp Biochem Physiol A 131:267–274

2. Mintun MA, Lundstrom BN, Snyder AZ, Vlassenko AG, Shulman GL, Raichle ME (2001) Blood flow and oxygen delivery to human brain during functional activity: theoretical modeling and experimental data. Proc Natl Acad Sci USA 98:6859–6864
3. Lindauer U, Gethmann J, Kühl M, Kohl-Bareis M, Dirnagl U (2003) Neuronal activity-induced changes of local cerebral microvascular blood oxygenation in the rat: effect of systemic hyperoxia or hypoxia. Brain Res 975:135–140
4. Sicard KM, Duong TQ (2005) Effects of hypoxia, hyperoxia, and hypercapnia on baseline and stimulus-evoked BOLD, CBF, and CMRO2 in spontaneously breathing animals. Neuroimage 25:850–858
5. Sukhotinsky I, Dilekoz E, Moskowitz MA, Ayata C (2008) Hypoxia and hypotension transform the blood flow response to cortical spreading depression from hyperemia into hypoperfusion in the rat. J Cereb Blood Flow Metab 28:1369–1376
6. Kanno I, Fujita H, Hatazawa J (1996) Enhancement of CBF response for VI stimuli during hyperoxia: behavior of oxygen in neuronal activation revisited. J Cereb Blood Flow Metab 17:S646
7. Kashikura K, Kershaw J, Kashikura A, Matsuura T, Kanno I (2000) Hyperoxia-enhanced activation-induced hemodynamic response in human VI: an fMRI study. Neuroreport 11:903–906
8. Duong TQ (2007) Cerebral blood flow and BOLD fMRI responses to hypoxia in awake and anesthetized rats. Brain Res 1135:186–194
9. Magistretti PJ, Pellerin L, Rothman DL, Shulman RG (1999) Energy demand. Science 22:496–497
10. Iadecola C (2004) Neurovascular regulation in the normal brain and in Alzheimer's disease. Nat Rev Neurosci 5:347–360
11. Matsuura T, Takuwa H, Bakalova R, Obata T, Kanno I (2009) Effect of cyclooxygenase-2 on the regulation of cerebral blood flow during neuronal activation in the rat. Neurosci Res 65:64–70
12. Iadecola C (1992) Does nitric oxide mediate the increases in cerebral blood flow elicited by hypercapnia? Proc Natl Acad Sci USA 89:3913–3916
13. Solfrizzi V, D'Introno A, Colacicco AM, Capurso C, Del Parigi A, Capurso S, Gadaleta A, Capurso A, Panza F (2005) Dietary fatty acids intake: possible role in cognitive decline and dementia. Exp Gerontol 40:257–270
14. Matsuura T, Kanno I (2001) Quantitative and temporal relationship between local cerebral blood flow and neuronal activation induced by somatosensory stimulation in rats. Neurosci Res 40:281–290
15. Matsuura T, Fujita H, Seki C, Kashikura K, Kanno I (1999) CBF change by somatosensory activation measured by laser-Doppler flowmetry: independent evaluation of RBC velocity and RBC concentration. Jpn J Physiol 49:289–296
16. Bakalova R, Matsuura T, Kanno I (2002) The cyclooxygenase inhibitors indomethacin and rofecoxib reduce regional cerebral blood flow evoked by somatosensory stimulation in rats. Exp Biol Med (Maywood) 227:465–473
17. Pelligrino DA, Wang Q, Koenig HM, Albrecht RF (1995) Role of nitric oxide, adenosine, *N*-methyl-D-aspartate receptors, neuronal activation in hypoxia-induced pial arteriolar dilation in rats. Brain Res 704:61–70
18. Matsuura T, Fujita H, Kashikura K, Kanno I (2000) Evoked local cerebral blood flow induced by somatosensory stimulation is proportional to the baseline flow. Neurosci Res 38:341–348
19. Packer L, Prilipko L, Christen Y (eds) (1992) Free radicals in the brain. Springer, Berlin

BRAIN RESEARCH 1354 (2010) 30–39

available at www.sciencedirect.com

ScienceDirect

www.elsevier.com/locate/brainres

BRAIN RESEARCH

Research Report

# Regional heterogeneity and age-related change in sub-regions of internal capsule evaluated by diffusion tensor imaging

*Hiroshi Kawaguchi*[a,*], *Takayuki Obata*[a], *Miho Ota*[b], *Yoshihide Akine*[b], *Hiroshi Ito*[b], *Hiroo Ikehira*[a], *Iwao Kanno*[a], *Tetsuya Suhara*[b]

[a]*Department of Biophysics, Molecular Imaging Center, National Institute of Radiological Sciences, Japan*
[b]*Department of Molecular Neuroimaging, Molecular Imaging Center, National Institute of Radiological Sciences, Japan*

ARTICLE INFO

*Article history:*
Accepted 23 July 2010
Available online 1 August 2010

*Keywords:*
Human internal capsule
Regional heterogeneity
Aging
Diffusion tensor imaging

ABSTRACT

The internal capsule (IC) includes various fiber tracts supporting sensory, motor and cognitive abilities. Diffusion tensor imaging (DTI) is useful for the diagnosis of brain diseases related to IC. However, there is some risk of misdiagnosis when measuring diffusion parameters throughout the whole IC without knowledge of age-related changes, as the thin structure and branching in multiple directions must be expected to produce sub-regional differences. In this study, regional heterogeneity and age-related changes in water diffusion parameters were evaluated in sub-regions of IC. The IC region-of-interest (ROI) was first thinned to reduce contamination from surrounding tissues and then morphologically divided into three regions: anterior limb (AL), genu and posterior limb (PL). To address the branching of PL, a procedure was applied to divide the thinned PL ROI into 10 equally-spaced positions. Estimates of fractional anisotropy (FA), mean diffusivity (MD), and longitudinal ($\lambda_L$) and transversal ($\lambda_T$) eigenvalues showed age-related and location-dependent variation in AL, genu and PL ROIs and at the 10 equally-spaced positions of PL. Simultaneous decrease of $\lambda_L$ and increase of $\lambda_T$ resulting in decrease of FA and steady MD with aging were observed. This might be caused by age-related atrophy of main fibers such as the pyramidal tract, possibly resulting in an increase in the relative signal contribution of some crossing fibers in each pixel. Evaluation using eigenvalues ($\lambda_L$ and $\lambda_T$), as well as FA and MD, may provide important information towards understanding age-related changes and may also be useful for clinical diagnosis of diseased IC.



## 1. Introduction

Diffusion tensor imaging (DTI) has been widely applied in a large number of studies to obtain clinically important information about axonal fibers in white matter (Le Bihan, 2007; Peled et al., 1998). In white matter, water motion is restricted in the directions perpendicular to the axons that are oriented along the fiber tracts. This anisotropic diffusion is due to the presence of tightly packed multiple myelin membranes encompassing the axon (Peled et al., 1998). DTI provides measurements of mean diffusivity (MD), the value representing the strength of the diffusion, and fractional (FA)

* *Corresponding author.* 4-9-1, Anagawa, Inage-ku, Chiba, 263-8555, Japan. Fax: +81 43 206 0819.
E-mail address: kwgc@nirs.go.jp (H. Kawaguchi).

*Abbreviations:* DTI, diffusion tensor imaging; FA, fractional anisotropy; MD, mean diffusivity; ROI, region-of-interest; RA, relative anisotropy; IC, internal capsule; AL, anterior limb; PL, posterior limb; VBM, voxel-based morphometry; TBSS, tract-based spatial statistics

0006-8993/$ – see front matter © 2010 Elsevier B.V. All rights reserved.
doi:10.1016/j.brainres.2010.07.084

or relative (RA) anisotropy, the index representing directionality, to describe water motion in tissue. DTI has also been used to study the degeneration of white matter with age. For example, in corpus callosum, where the fiber direction is mostly one-way, results have suggested that degeneration of the fiber tract with age can produce an increase of MD and decrease of FA due to the loss of myelin and axonal membranes (Ota et al., 2006). Variation of the diffusion parameters with age must be clarified in normal volunteers before DTI can be used for clinical diagnosis of fiber-tract abnormality (Moseley, 2002).

Changes to the diffusion tensor of water in the internal capsule (IC) are potentially useful for the diagnosis of various brain diseases, such as dementia, metabolic brain disorders and developmental diseases, and also in the follow-up after ischemia. However, there is some risk of misdiagnosis when measuring diffusion parameters throughout the whole IC. IC contains many axonal fiber connections relating to sensory, motor and cognitive abilities and branching in various directions between tissues in the brain (Wolf-Heidegger and Köpf-Maier, 2000; Zarei et al., 2007). Furthermore, fiber tracts coexist with orientations in different directions, and the composition ratio and directions vary depending on the anterior–posterior position in IC (Axer and Keyserlingk, 2000). IC is often morphologically divided into three regions: anterior limb (AL), genu and posterior limb (PL). AL contains anterior thalamic radiation and frontopontine fibers. The genu contains corticonuclear fibers connected to the head and neck muscles. The anterior two-thirds of PL contains corticospinal fibers for muscles of the upper limbs, chest wall, abdominal wall and lower limbs, while the posterior third contains thalamoparietal fibers, temporopontine fibers, acoustic and optic radiation. From these details, it would be prudent to analyze the results of DTI of IC in terms of the separate sub-regions rather than as a whole.

Thus, understanding the normal age-related DTI changes and differences among IC sub-regions is crucial for an accurate diagnosis. This kind of detailed approach may provide important information concerning the relationship between the brain cortex and basal ganglia or spinal cord. There have been several reports concerning IC and aging measured with DTI by region-of-interest (ROI) analysis (Abe et al., 2002; Ardekani et al., 2007; Bhagat and Beaulieu, 2004; Furutani et al., 2005; Hsu et al., 2008; Madden et al., 2004; Salat et al., 2005; Sullivan et al., 2010). Whole-brain analysis such as by voxel-based morphometry (VBM) (Ardekani et al., 2007; Furutani et al., 2005; Hugenschmidt et al., 2008; Nusbaum et al., 2001; Pagani et al., 2008; Salat et al., 2005) and tract-based spatial statistics (TBSS) (Smith et al., 2006; Burzynska et al., 2010; Kochunov et al., 2007; Vernooij et al., 2008) has also been employed for the investigation of age-related changes of IC. However, the results of those studies were inconsistent, especially in age-related change of diffusion anisotropy in PL (for details, see Discussion), perhaps due to partial volume contamination from surrounding tissues and sub-regional differences in the fiber tracts. Previous reports have shown that misalignment and partial volume contamination from surrounding tissue caused by spatial smoothing can affect the results (Ardekani et al., 2007; Snook et al., 2007). It is necessary to evaluate the age-related change in diffusion parameter estimates by reducing the influence of the partial volume effect and detecting the tendency of various fiber tracts as accurately as possible.

The aim of the present study was to show the age-related change of sub-regions in IC by reducing the influence of partial volume contamination as much as possible. The IC was outlined on individual FA images, and then the outlined mask was thinned to reduce partial volume contamination. IC was morphologically divided into three regions: AL, genu and PL, and age-related changes of the diffusion parameter estimates of adult human were investigated. Moreover, PL was divided into 10 equally-spaced positions because of the heterogeneous component, as mentioned above. To the best of our knowledge, this kind of detailed approach has not been reported in the literature. The results obtained by our procedure were compared with those obtained by the VBM procedure, to show how partial volume contamination affects the diffusion parameter estimates and age-related change of the estimates in IC.

## 2. Results

### 2.1. *Comparison of FA values between before and after thinning*

Fig. 1 shows the scatter plot for evaluating the effect of thinning for the whole IC ROI in either hemisphere. The averaged FA value after thinning was obviously greater than that before thinning for every subject. The difference before and after thinning was statistically significant by evaluation with Wilcoxon signed rank test ($p<0.01$).

### 2.2. *Regional heterogeneities of IC sub-regions and comparison with VBM*

Table 1 shows the multiple group comparison for sub-regional differences of diffusion parameter estimates on original

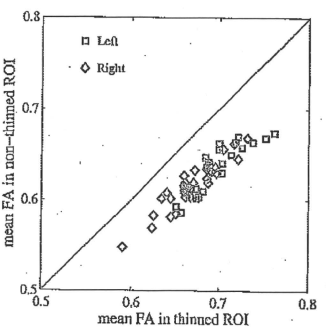


**Fig. 1 – Scatter plot of the FA values averaged in thinned ROI and regional mask of whole internal capsule to evaluate the reduction of partial volume effect. The detailed definition of thinned ROI and regional mask is shown in Fig. 5.**

Table 1 – Comparison of positional difference of diffusion parameter estimates for the anterior limb (AL), genu and posterior limb (PL) of the internal capsule on the bilateral thinned ROIs on original individual images (Friedman's test, degree of freedom: 5, 25). L and R correspond to left and right, respectively. The significance (p) indicates that there is a group-wise positional difference in each parameter estimate.

| | FA | MD | $\lambda_L$ | $\lambda_T$ |
|---|---|---|---|---|
| $\chi^2$ | 102.418 | 54 | 61.6264 | 94.5275 |
| p | <0.01 | <0.01 | <0.01 | <0.01 |

images (neither normalization nor smoothing) by Friedman's test (degree of freedom: 5, 25). The thinned IC on individual original images was divided to 6 sub-regions; left and right AL, genu and PL. In addition to FA and MD, $\lambda_L$ (longitudinal or maximum eigenvalue) and $\lambda_T$ (transversal eigenvalue; average of the 2nd and 3rd eigenvalues) were also calculated. The regional differences were detected on every diffusion parameter estimate.

Fig. 2 shows the influence of spatial normalization and smoothing on the diffusion parameter estimates of the six IC sub-regions. In the VBM procedure, the ROIs were located on the normalized template and the diffusion parameter estimates were sampled on normalized and smoothed images for each subject. FA and $\lambda_L$ of all regions on original images were greater than those on VBM images. $\lambda_T$ of all regions on original images was smaller than that on VBM image.

### 2.3. *Age-related changes of IC sub-regions and comparison with VBM*

Spearman's correlation coefficients were calculated from both the data of original and VBM images and summarized in Table 2. The scatter plots of age versus diffusion parameter estimates of the data from original images are shown in Fig. 3. FA and $\lambda_L$ showed age-related decline in all regions in the data from both individual and VBM images. However, all correlation coefficients of FA from original images were greater than those from VBM images except for left PL. FA had a significant negative correlation with age for AL in both hemispheres (left: $\rho=-0.49$, $p=0.012$; right: $\rho=-0.62$, $p=0.001$) and for the right genu ($\rho=-0.43$, $p=0.027$) and PL ($\rho=-0.40$, $p=0.041$) in the data from original images, but it had correlation only for PL ($\rho=-0.39$, $p=0.047$) in the data from VBM images. MD was not significantly correlated with age for any of the regions in the data from original images, but it showed a significant positive correlation for left AL ($\rho=-0.42$, $p=0.031$) in the data from VBM images. $\lambda_L$ had a significant negative correlation with age for the right AL ($\rho=-0.58$, $p=0.002$) in the data from original images, while it had correlation for the left AL ($\rho=-0.41$, $p=0.039$) in VBM images. $\lambda_T$ showed age-dependent increase in all regions, and a significant positive correlation for the right AL (on original images, $\rho=0.56$, $p=0.003$; on VBM images, $\rho=0.44$, $p=0.026$).

### 2.4. *Diffusion parameter estimates in 10 equally-spaced anterior to posterior positions of PL*

Results for the 10 equally-spaced anterior to posterior positions of PL are shown in Fig. 4. All diffusion parameter estimates varied significantly depending on their position within PL, indicating the need to divide PL into sub-regions for evaluation of IC (Table 3). While FA showed age-related decline in all regions, the trend of this decline was greater on the right than on the left side. FA had a significant age-related negative correlation at the 8th position on the right ($\rho=-0.41$, $p=0.036$). Regarding PL in both hemispheres, MD showed an age-related increase near the genu (position 1), then a decline followed by an increase as the position moved towards the posterior edge. MD only had a significant

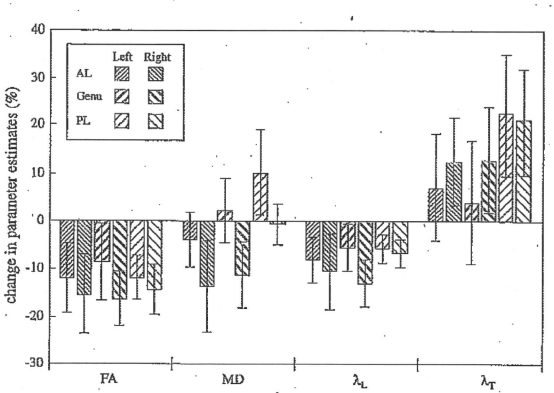


**Fig. 2 – The percentage difference in diffusion parameter estimates for the anterior limb (AL), genu and posterior limb (PL). The height of the bars represents the percent difference of the estimates from original image to VBM image (e.g. $(FA_{norm}-FA_{org})/FA_{org}$). The error bar shows standard deviation between subjects.**

Table 2 – Dependence of diffusion parameter estimates on age in the thinned ROI of anterior limb (AL), genu and posterior limb (PL) of internal capsule. Spearman's correlation coefficients were calculated on the data from ROIs defined on the average of spatially-normalized (VBM) image ($\rho_{norm.}$) and on original images ($\rho_{org.}$), respectively. A p-value of less than 0.05 was considered significant and is indicated by boldface.

| | ROI | | $\rho_{norm.}$ (p-value) | $\rho_{org.}$ (p-value) | | ROI | | $\rho_{norm.}$ (p-value) | $\rho_{org.}$ (p-value) |
|---|---|---|---|---|---|---|---|---|---|
| FA | AL | L | −0.39 (0.047) | −0.49 (0.012) | $\lambda_L$ | AL | L | −0.41 (0.039) | −0.36 (0.059) |
| | | R | −0.32 (0.110) | −0.62 (0.001) | | | R | −0.08 (0.713) | −0.58 (0.002) |
| | Genu | L | −0.11 (0.596) | −0.31 (0.129) | | Genu | L | −0.34 (0.084) | −0.20 (0.334) |
| | | R | −0.37 (0.059) | −0.43 (0.027) | | | R | −0.32 (0.114) | −0.13 (0.523) |
| | PL | L | −0.21 (0.303) | −0.15 (0.453) | | PL | L | −0.41 (0.040) | −0.34 (0.093) |
| | | R | −0.24 (0.228) | −0.40 (0.041) | | | R | −0.16 (0.426) | −0.18 (0.373) |
| MD | AL | L | 0.42 (0.031) | −0.03 (0.873) | $\lambda_T$ | AL | L | 0.38 (0.054) | 0.35 (0.082) |
| | | R | 0.31 (0.118) | 0.02 (0.913) | | | R | 0.44 (0.026) | 0.56 (0.003) |
| | Genu | L | −0.25 (0.226) | 0.05 (0.814) | | Genu | L | 0.06 (0.778) | 0.22 (0.291) |
| | | R | 0.17 (0.415) | 0.19 (0.363) | | | R | 0.30 (0.141) | 0.35 (0.082) |
| | PL | L | −0.29 (0.153) | −0.24 (0.246) | | PL | L | 0.10 (0.628) | 0.08 (0.696) |
| | | R | 0.16 (0.432) | 0.18 (0.383) | | | R | 0.19 (0.364) | 0.36 (0.069) |

negative correlation with age at the 4th position on the left-hand side ($\rho$=−0.46, p=0.019). $\lambda_L$ had negative correlation with age at almost all positions, but significant negative correlation was only observed at the 2nd to 4th positions on the left side (2nd: $\rho$=−0.51, p=0.007; 3rd: $\rho$=−0.47, p=0.016; 4th: $\rho$=−0.51, p=0.007) and at the 3rd position on the right side ($\rho$=−0.41, p=0.039). $\lambda_T$ had positive correlations with age at almost all positions, but they were not statistically significant. The increasing trend of $\lambda_T$ with age was greater on the right than on the left side.

## 3. Discussion

### 3.1. *Methodological considerations*

The two most common methods used when comparing across subjects are ROI-based analysis and VBM. As discussed in previous reports, both methods have advantages and disadvantages (Ardekani et al., 2007; Salat et al., 2005; Smith et al., 2006; Snook et al., 2007). ROI-based analysis can be used to compare the parameter estimates at the same anatomic position when determined by an experienced operator. However, it can take a long time to analyze a large number of subjects, and the result can include some arbitrariness. The strength of VBM is that it estimates the parameters voxel-by-voxel throughout the whole brain for each subject. Unfortunately, there is no guarantee that, after registration with a standard template, the signal of a voxel comes from the same anatomical tissue for each subject. Although spatial smoothing can reduce the influence of misalignment on spatial normalization, it also increases the partial volume effect. As shown in Fig. 2 and Table 2, spatial adjustment affects not only the values of the diffusion parameter estimates but also the age-related change of those parameters.

A new alternative method, TBSS, has been proposed to address these problems (Smith et al., 2006). TBSS combines the strength of VBM with ROI-based analysis. The concept of spatial comparison across subjects is similar between the method we applied and TBSS; that is, the parameter estimates were evaluated on the skeleton of white matter so that it only contained pixels having a pure IC signal. While TBSS makes a skeleton on the mean FA image and analyzes the highest value on a line perpendicular to the skeleton on individual FA images, our procedure makes a skeleton on individual FA images. Unfortunately, it was not possible to apply TBSS to our data because we used a lower b-value than that suggested for acquisition (Smith et al., 2007). Furthermore, there is no way to prove which method is better for evaluating inter-subject comparison from the point of view that data came from anatomically identical positions of IC among all subjects, because the cell-level structures of IC may differ among individuals.

The width of IC in the left–right direction is narrow (a few pixels in the present study), which means that diffusion parameter estimates can easily be influenced by the properties of surrounding tissues such as the thalamus, globus pallidus and striatum with quite different cell-level structures from IC. As shown in Fig. 1, the averaged FA after thinning is obviously greater than that before thinning. The result principally reflects that the thinning can reduce the partial volume effect from surrounding gray matter that has a considerably lower FA value than white matter. Although regional heterogeneity of IC may affect the result, the influence was supposedly smaller than the reduction of the partial volume effect, as a microscopic study did not report a difference in axonal structure in the left–right direction in IC (Axer and Keyserlingk, 2000). In this study, we also selected ROIs from individual FA images without applying spatial smoothing because the process can mix the signal from IC and surrounding tissues. This may explain why FA of the present study was greater than those of some previous reports, thereby indicating that our method could reduce signal contamination of surrounding gray matter, which has lower FA than white matter. Although our approach is time-consuming and requires considerable effort to define the ROI (and may include some arbitrariness), we believe that it is a useful method for analyzing IC because it avoids the aforementioned problems.

Statistical analysis may affect the result. In this study, non-parametric statistics was used to evaluate age-related changes in the diffusion parameters, whereas in other

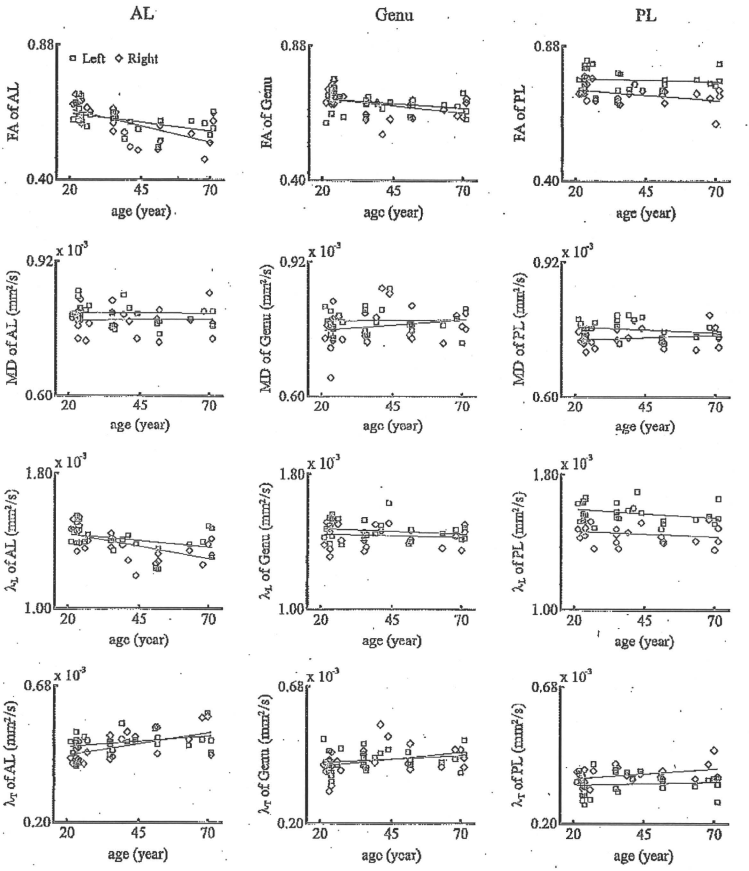


**Fig. 3 – Scatter plots of the diffusion parameter estimates vs. age for the anterior limb (AL), genu and posterior limb (PL) of the internal capsule on the bilateral thinned ROIs. Note that the regression line was just drawn to show the trend of increase or decrease of the parameter estimates with aging.**

studies parametric methods are most often used. The reason for choosing non-parametric statistics was that the diffusion parameters have a limited range of values ($0 \leq FA \leq 1$ and MD, $\lambda_L$ and $\lambda_T > 0$), meaning that there is no guarantee that the sampled data are normally distributed.

### 3.2. *Regional heterogeneity in IC*

The heterogeneous fiber orientation in IC was well established by a postmortem study using confocal and polarized microscopy (Axer and Keyserlingk, 2000). Although it is difficult to define all of the fibers passing through IC by DTI because of their crossing and complexity (Zarei et al., 2007), the diffusion parameter estimates can reflect information related to cell-level structures. The postmortem study showed that the anterior thalamic peduncle and fronto-pontine tracts were located in the posterior two-thirds of AL and that the angle between the two tracts varied from 60 to 70°, which can explain the lower FA in AL than that in PL (Fig. 3). The present data also showed regional heterogeneity between sub-regions of PL (Fig. 4 and Table 3). Along the anterior–posterior direction of PL, the averaged

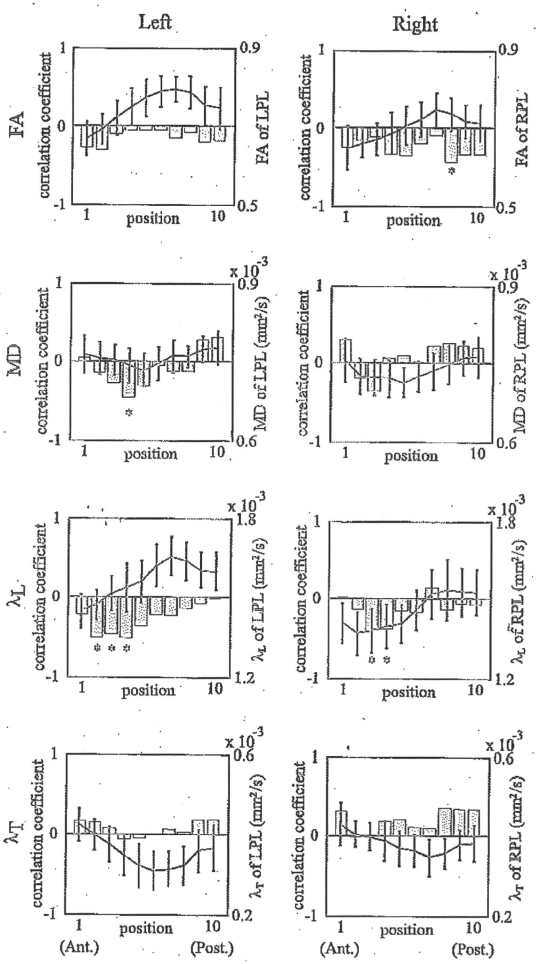


**Fig. 4 – Correlation between diffusion parameter estimates and age for the 10 equally-spaced positions of the posterior limb of the internal capsule. Bars indicate correlation coefficients and correspond to the left vertical axis. The line graphs are the averaged diffusion parameter estimates ± standard deviation and correspond to the right vertical axis. Positions 1 and 10 correspond to the most anterior and posterior points, respectively. * indicates statistically significant difference ($p<0.05$).**

FA value across subjects was increased, reaching a maximum at the 7th position, and then decreased. This tendency agrees well with the postmortem study, which showed that the pyramidal tract was located in the anterior position of PL intermingled with fibers of the superior thalamic peduncle, the intermingled proportion of the two tracts continued to decrease in the anterior–posterior direction, and the fiber orientation was heterogeneous in the posterior part of PL. The sub-regional analysis of diffusion parameter estimates along the anterior–posterior direction of PL can help the localization of a specific tract and diagnosis of the clinical state.

Table 3 – Comparison of diffusion parameter estimates among 10 equally-spaced positions in the posterior limb (Friedman's test, degree of freedom: 9, 25). The significance (p) indicates that there is a group-wise positional difference in each parameter estimate.

| | FA | | MD | | $\lambda_L$ | | $\lambda_T$ | |
|---|---|---|---|---|---|---|---|---|
| | L | R | L | R | L | R | L | R |
| $\chi^2$ | 153.71 | 112.62 | 46.79 | 62.73 | 156.99 | 121.92 | 131.17 | 78.42 |
| p | <0.01 | <0.01 | <0.01 | <0.01 | <0.01 | <0.01 | <0.01 | <0.01 |

There was statistically significant laterality in $\lambda_L$ of PL in the data from original images (data not shown). It is difficult to comment on the relationship between handedness and the data because the subjects were right-handers only. It will be necessary to measure left-handers in order to draw any conclusions on the difference and handedness.

### 3.3. *Age-related change in IC*

The present data showed an age-related decline of FA in all sub-regions of IC, and bilateral AL and right genu and PL showed statistical significance. Age-related FA decline in AL was reported in previous studies using ROI-based analysis or TBSS (Burzynska et al., 2010; Ardekani et al., 2007; Hsu et al., 2008), but two ROI-based studies suggested no change (Bhagat and Beaulieu, 2004; Madden et al., 2004). As the latter used comparatively large ROI and thick slices, the averaging of FA values in ROI and the partial volume effect from surrounding gray matter might weaken the age-related change in AL. FA decline in AL was not found in any of the VBM studies. A non-negligible number of studies have reported age-related FA increase in the striatum (Abe et al., 2008; Bhagat and Beaulieu, 2004; Camara et al., 2007; Hasan et al., 2008), indicating why no age-related change in AL was found in previous VBM studies using spatial smoothing. Age-related decline in PL was reported in studies using each of VBM (Ardekani et al., 2007; Hsu et al., 2008; Salat et al., 2005), TBSS (Burzynska et al., 2010), and ROI-based analysis (Bhagat and Beaulieu, 2004). Although Abe et al. reported no statistically significant age-related change of FA in PL using ROI-based analysis, they speculated that their large ROI might have suppressed the change (Abe et al., 2002). Some studies using VBM did not find age-related change of FA in PL (Camara et al., 2007; Hugenschmidt et al., 2008; Pagani et al., 2008), and a VBM study showed an inexplicable significant partial increase and decline of RA in PL (Nusbaum et al., 2001). As mentioned above, differences in technique for inter-subject comparison strongly affect the results of the analysis of age-related change in PL, which at least suggests the risk of using VBM to evaluate age-related change in IC.

The present data did not indicate an age-related change of MD. Previous studies have reported that MD did not show any age-related change (Abe et al., 2002) and showed a significant increase in AL (Ardekani et al., 2007), a slight increase in genu (Sullivan et al.), a significant decrease in PL (Camara et al., 2007), and a significant increase in AL and decrease in PL (Burzynska et al., 2010). Because of the inconsistency of these results, any conclusive statement regarding change of MD in IC remains problematic. Finally, MD may not be a suitable indicator of age-related change in IC. Possible reasons, besides partial volume effect, for the discrepancies between the present results and the several previous studies are: 1) differences in methodology to select the ROI, 2) misalignment of spatial normalization, 3) differences in statistical analysis (e.g. parametric vs. non-parametric), 4) differences in the number and age range of subjects, and 5) differences in slice thickness. The present study found a statistically significant decline in $\lambda_L$ and a statistically significant increase in $\lambda_T$ in the right AL and slight decline in $\lambda_L$ and a slight increase in $\lambda_T$ in the other sub-regions. This tendency agrees well with the previous report using TBSS (Burzynska et al., 2010). It seems that $\lambda_L$ and $\lambda_T$ may be more stable indicators for age-related degeneration.

The simultaneous increase of MD and decrease of FA are usually associated with aging in white matter (Ardekani et al., 2007; Ota et al., 2006; Sullivan et al., 2010). However, the present results did not show this tendency. It has been suggested that the decline in FA is related to the increase in $\lambda_T$, which is attributable to the age-related decrease of cell density (Le Bihan, 2007). The present results showed not only an increase in $\lambda_T$, but also a decrease in $\lambda_L$, which may be the reason for the smaller age-related change of MD in this study. This tendency is somewhat prominent in AL and the anterior regions of PL, where corticothalamic fibers intermingle with the main tract such as cortico-spinal and cortico-pontine tracts (Axer and Keyserlingk, 2000). The age-related changes of diffusion parameter estimates may be affected by secondary Wallerian degeneration, gliosis and/or early axonal injury (Burzynska et al., 2010). As another speculation, supposing that corticothalamic fibers are relatively spared from age-related change compared to cortico-spinal and cortico-pontine tracts, atrophy of cortico-spinal and cortico-pontine tracts and subsequent contamination by corticothalamic fibers intruding into the atrophied space may restrict water diffusion in the principal direction, thereby causing the age-related decline of $\lambda_L$. This suggests that decreases in $\lambda_L$, which are not observed in the corpus callosum with a well-oriented fiber structure, should be considered during diagnosis of the IC structure with DTI.

### 3.4. *Limitation*

Statistical significance of the correlation between diffusion parameter estimates and age is strongly influenced by the size (n) of the study group. It is possible that an increase in the number of subjects would increase the statistical power of the present results. Inter-subject analysis was applied to the thinned ROI to reduce the partial volume effect and anatomically compare the same position as accurately as possible. However, it is not definite that the present data came from anatomically identical positions of IC among all the subjects, since the cell-level structures of IC may differ between individuals. Long-term monitoring of the same subjects will contribute to explicating the precise aging effect in IC.

### 3.5. Concluding remarks

Age-related changes in diffusion parameter estimates were evaluated for thinned ROIs defined in sub-regions of IC. The diffusion parameters and age-related changes showed a dependence on position for the 10 equally-spaced positions of PL, indicating that the often used ROI-based method may overlook characteristic parameter changes in small regions. IC is the narrow region in the left–right direction and is surrounded by the basal nucleus where the tissue diffusion properties are quite different from those of IC. Thus, VBM may produce incorrect results caused by partial voluming with surrounding tissues. This type of contamination was avoided in our work by applying a procedure to thin the individually-selected ROIs. Our results did not find the simultaneous increase of MD and decrease of FA that are usually observed with respect to aging in other white matter. This may be related to the directional dependency of fiber-tract atrophy that was suggested by the age-related changes in $\lambda_L$ and $\lambda_T$. Evaluation using not only FA and MD, but also $\lambda_L$ and $\lambda_T$, may help the understanding of age-related alterations and may also be useful for clinical diagnosis of brain diseases that affect water motion in IC.

## 4. Experimental procedures

### 4.1. Participants

Twenty-six healthy men (right-handed; mean age: 39.3± 17.5 years, ranges: 21–39 years, n=16; 40–59, n=5; 60–71, n=5) participated in this study. The participants partially overlapped with those in two previous studies (Ota et al., 2006; Ota et al., 2007). Anatomical MR images were acquired prior to the experiment to rule out morphological brain abnormalities. All subjects were without neurological illness, head trauma, loss of consciousness, or psychiatric disorder. The study was approved by the Ethics and Radiation Safety Committees of the National Institute of Radiological Sciences, Chiba, Japan. All participants gave their written informed consent.

### 4.2. DTI data acquisition and estimation of diffusion parameters

Images were acquired using a Philips Intera 1.5 Tesla MR unit (Philips Medical Systems, Best, The Netherlands). MR data acquisition and DTI calculations were performed in the same manner as described in previous work (Ota et al., 2006). Diffusion-weighted images were acquired by single-shot echo-planar imaging with the sensitivity-encoding (SENSE) parallel-imaging scheme (reduction factor=2.0, TR=8645 ms, TE=96 ms). The field-of-view was 240×240 mm$^2$ (nominal resolution, 2.5 mm) with an imaging matrix of 96×96 zero-filled to 256×256 pixels. Sixty continuous transverse slices were acquired with 2.5-mm slice thickness, and b-values of 0 s/mm$^2$ and 700 s/mm$^2$. Diffusion was measured along six non-collinear directions: (x, y, z)=[(1, 0, 0), (0, 1, 0), (0, 0, 1), (−0.707, 0.707, 0), (0.707, 0, −0.707), (0, 0.707, −0.707)]. Acquisition was repeated 30 times to enhance the signal-to-noise ratio, and the total scan time was 40 min. Each directional volume from the diffusion data set was re-sampled to the b=0 image to correct for remaining eddy current distortion (Kim et al., 2002) as well as to correct for participant motion. Dtistudio (H. Jaing, S. Mori; Johns Hopkins University) was used to analyze MR data sets. The six components of the apparent diffusion tensor were calculated at each voxel from the b=0 and six diffusion-weighted (b=700) images. Eigenvalues and eigenvectors were obtained by diagonalization of the estimated diffusion tensors. FA, MD, $\lambda_L$ (longitudinal or maximum eigenvalue) and $\lambda_T$ (transversal eigenvalue; average of the 2nd and 3rd eigenvalues) were calculated on a voxel-by-voxel basis. To clarify the influence of spatial normalization and smoothing on the results, these values were also calculated on images normalized to the stereotactic template using statistical parametric mapping (SPM2) (Wellcome Department of Imaging Neuroscience, London, UK). The detailed procedure for spatial transformation was described in our previous report (Ota et al., 2007). Non-diffusion-weighted (b=0) image was first normalized to the Montreal Neurological Institute 152-subject T2 template, and then the transformation matrix was applied to the images of diffusion parameter estimates to normalize them to the stereotactic space. Finally, each image was spatially smoothed by 5-mm full-width at half maximum Gaussian kernel that was empirically used for functional MRI and positron emission tomography studies (Snook et al., 2007).

### 4.3. ROI definition

IC is the narrow region in the left–right direction and is surrounded by several different types of basal ganglia. Thus, the selected ROI may be affected by the partial volume effect, especially at the edge pixels. We used a thinned ROI to alleviate this problem. The ROI definition is shown in Fig. 5. The thinned ROI was created in two steps. First, one operator (HK) drew a boundary around the IC in both hemispheres on individual non-warped FA images (Fig. 5b) and the average of warped FA images. Axial slices between the anterior commissure and superior boundary of the lenticular nucleus were used for masking (5 or 6 slices per subject) to select the anatomically equivalent region among subjects. The mask was defined by using the globus pallidus, the head of the caudate nucleus and the thalamus as regional landmarks. The anterior boundary of the ROI was defined by the anterior edges of the globus pallidus and caudate nucleus, and the posterior boundary by the posterior edges of the globus pallidus and thalamus. A national-board-certified radiologist (TO) checked and corrected the anatomical mask position. In the second step, the mask was thinned with a robust thinning algorithm to reduce possible partial volume effects (Fig. 5c) (Telea and van Wijk, 2002). Thereafter, IC was divided into three regions, i.e., AL, genu and PL. The one or two pixels where the thinned ROI changed directions were taken as the genu, with the remaining anterior and posterior pixels forming AL and PL regions, respectively (Fig. 5d). The above procedures were also applied to the original individual images and the averaged VBM images of all subjects for each

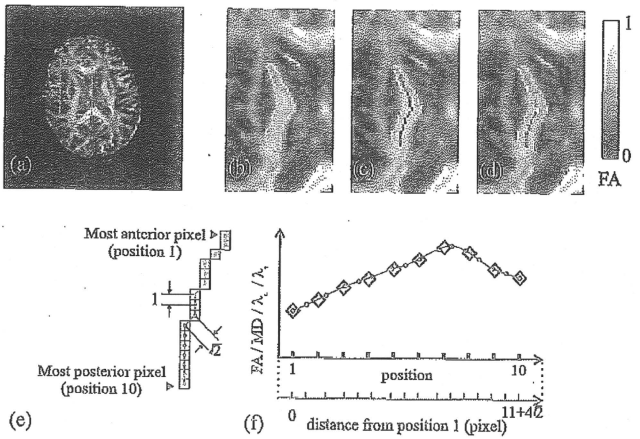


**Fig. 5 – Process used to define the region-of-interest in the internal capsule. (a) Fractional anisotropy image from a typical subject. The green line indicates the boundary of figures (b)–(d). (b) Mask of the internal capsule (red line). (c) Thinned region-of-interest (ROI) (blue line). (d) Sub-regions of the internal capsule; anterior limb (cyan), genu (yellow), and posterior limb (PL) (magenta). (e) Magnified example of a thinned PL ROI. (f) The parameter estimates at each pixel in the ROI were plotted on an axis (from first to last) according to the distance between pixel centers (closed purple circles and scale). The axis was then divided into 10 equally-spaced positions and interpolated values for the parameters were calculated at those positions (open black diamonds and scale). (For interpretation of the references to color in this figure legend, the reader is referred to the web version of this article.)**

of the diffusion parameter estimates. Following the procedure described in Figs. 5e–f, the PL ROI was then divided into 10 equally-spaced positions and the diffusion parameters were re-sampled at these positions using shape-preserving piece-wise cubic interpolation.

### 4.4. *Statistical analysis*

Statistical analyses were performed with custom Matlab (Mathworks, Natick, MA) scripts. FA, MD and the eigenvalues were averaged over the AL, genu and PL ROIs. To assess the need to divide IC and PL ROI, Friedman's test was applied. Then, dependence of the averaged values on age was evaluated across subjects using Spearman's correlation coefficient. The age dependence of the re-sampled estimates of the 10 equally-spaced positions in the PL ROI was assessed across subjects in the same way. A p-value of less than 0.05 was considered significant.

## Acknowledgments

We thank Mr. Jeff Kershaw for important suggestions and comments. This work was supported in part by a Grant-in-Aid from the Ministry of Education, Science, Sports and Culture of Japan, and KAKENHI from the Japan Society for the Promotion of Science.

## REFERENCES

Abe, O., Aoki, S., Hayashi, N., Yamada, H., Kunimatsu, A., Mori, H., Yoshikawa, T., Okubo, T., Ohtomo, K., 2002. Normal aging in the central nervous system: quantitative MR diffusion-tensor analysis. Neurobiol. Aging 23, 433–441.

Abe, O., Yamasue, H., Aoki, S., Suga, M., Yamada, H., Kasai, K., Masutani, Y., Kato, N., Ohtomo, K., 2008. Aging in the CNS: comparison of gray/white matter volume and diffusion tensor data. Neurobiol. Aging 29, 102–116.

Ardekani, S., Kumar, A., Bartzokis, G., Sinha, U., 2007. Exploratory voxel-based analysis of diffusion indices and hemispheric asymmetry in normal aging. Magn. Reson. Imaging 25, 154–167.

Axer, H., Keyserlingk, D.G., 2000. Mapping of fiber orientation in human internal capsule by means of polarized light and confocal scanning laser microscopy. J. Neurosci. Meth. 94, 165–175.

Bhagat, Y.A., Beaulieu, C., 2004. Diffusion anisotropy in subcortical white matter and cortical gray matter: changes with aging and the role of CSF-suppression. J. Magn. Reson. Imaging 20, 216–227.

Burzynska, A.Z., Preuschhof, C., Backman, L., Nyberg, L., Li, S.C., Lindenberger, U., Heekeren, H.R., 2010. Age-related differences in white matter microstructure: region-specific patterns of diffusivity. Neuroimage 49, 2104–2112.

Camara, E., Bodammer, N., Rodriguez-Fornells, A., Tempelmann, C., 2007. Age-related water diffusion changes in human brain: a voxel-based approach. Neuroimage 34, 1588–1599.

Furutani, K., Harada, M., Minato, M., Morita, N., Nishitani, H., 2005. Regional changes of fractional anisotropy with normal aging